Quantum Dot Luminescent Concentrator Cavity Exhibiting 30-fold Concentration

Noah D. Bronstein,[†,¶] Yuan Yao,[‡,¶] Lu Xu,[‡,¶] Erin O'Brien,[†] Alexander S. Powers,[†] Vivian E. Ferry,[§] A. Paul Alivisatos,[*,†,∥,⊥] and Ralph G. Nuzzo[*,‡,#]

[†]Department of Chemistry and [∥]Kavli Energy NanoScience Institute, University of California, Berkeley, California 94720, United States

[‡]Department of Chemistry, Frederick Seitz Materials Research Laboratory, and [#]Department of Materials Science and Engineering, University of Illinois at Urbana−Champaign, Urbana, Illinois 61801, United States

[§]Department of Chemical Engineering and Materials Science, University of Minnesota, Minneapolis, Minnesota 55455, United States

[⊥]Materials Science Division, Lawrence Berkeley National Laboratory, Berkeley, California 94720, United States

S *Supporting Information*

ABSTRACT: Luminescent solar concentrators doped with CdSe/CdS quantum dots provide a potentially low-cost and high-performance alternative to costly high-band-gap III−V semiconductor materials to serve as a top junction in multijunction photovoltaic devices for efficient utilization of blue photons. In this study, a photonic mirror was coupled with such a luminescent waveguide to form an optical cavity where emitted luminescence was trapped omnidirectionally. By mitigating escape cone and scattering losses, 82% of luminesced photons travel the length of the waveguide, creating a concentration ratio of 30.3 for blue photons in a waveguide with a geometric gain of 61. Further, we study the photon transport inside the luminescent waveguide, showing unimpeded photon collection across the entire length of the waveguide.

PL escapes ⟶ trapped with mirror
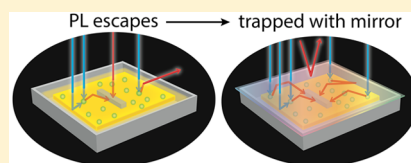
KEYWORDS: *luminescent solar concentrators, quantum dots, photovoltaics, transfer printing, light trapping*

L uminescent solar concentrators[1−4] (LSCs) have been studied extensively for the last three decades as low-cost alternatives to single- and multijunction photovoltaic (PV) devices. As silicon prices have fallen, it has become increasingly clear that future solar panels will need to have both low cost and high efficiency. One promising strategy for achieving a higher efficiency is to use different parts of the solar spectrum in photovoltaic materials with varying band gaps to minimize losses associated with carrier thermalization and incomplete photon absorption. For these multijunction (MJ) PV devices, there is a strong need for developing low-cost, high-band-gap solar cells for efficient utilization of the high-energy part of the solar spectrum. A luminescent solar concentrator could provide exactly this function, serving as the top junction in a multijunction architecture by converting blue photons into guided luminescence. Due to the concentration effect, only small amounts of high-performing but expensive III−V photovoltaic materials are needed to collect the light from an inexpensive luminescent waveguide. Such a device requires high concentration factors to reduce the cost of the III−V photovoltaic material. High concentration also allows the Stokes shift of the lumophore to be recovered in the operating voltage of the photovoltaic cell.

The concentration factor and collection efficiency achieved by LSCs to date have been limited due to parasitic losses such as nonunity quantum yields of the lumophores, imperfect light trapping within the waveguide, and reabsorption and scattering

of propagating photons.[5] Previous studies have sought to solve each of these parasitic losses individually, resulting in modest performance improvements.[6−15] Here we achieve a luminescent concentration ratio greater than 30 with an optical efficiency of 82% for blue photons by simultaneously addressing the materials and optical challenges of the LSC system. These concentration ratios are achieved through the combination of designer quantum dot lumophores and photonic mirrors, and microscale silicon photovoltaic cells are used to detect the concentration of light in the waveguide. To the best of our knowledge, this is the highest luminescent concentration factor in literature to date. Previously, a concentration factor of 22 was reported in 1984 by Roncali and Garnier[12,16] using a dye with high luminescence quantum yield in a highly polished waveguide with mirrored edges. Such a strategy resulted in a low waveguide efficiency due to unmitigated escape cone losses. In contrast, our use of photonic mirrors that are carefully matched to narrow bandwidth emitting quantum dot lumophores allowed us to achieve waveguide efficiency exceeding the limit imposed by total internal reflection. Lessons learned from our design offer guidance toward the development of devices with both high concentration factors and high collection efficiencies.
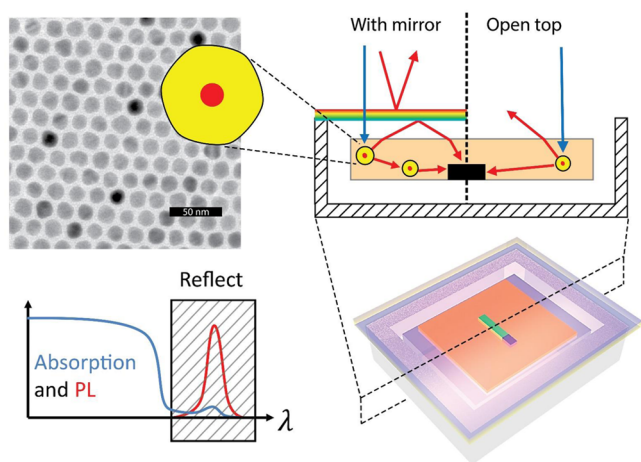
Figure 1. Graphic showing a typical transmission electron micrograph and schematic of giant CdSe/CdS quantum dots, incorporated into a traditional luminescent solar concentrator (open top) and the luminescent concentrator cavity (with mirror). The black rectangle is a photovoltaic cell. The blue arrows represent solar photons, which are then converted to red light by the quantum dots and either collected by the solar cell or lost to the escape cone. In the new design, a wavelength-selective mirror traps the luminescence inside the cavity, increasing the intensity of red light inside the cavity. The desired absorption, photoluminescence (PL), and reflectance spectra are sketched. The result is improved collection efficiency of red photons, which cannot escape, and improved power output from the solar cell.

The general principle behind LSCs is illustrated in Figure 1: broadband photons from the sun are absorbed by lumophores in a waveguide, and the emitted photons are guided via total internal reflection (TIR) to an adjacent solar cell, where they are converted to electricity. The thermodynamic limit of the concentration ratio (C), the ratio of the photon fluxes at the absorption energy (E_1), and emission energy (E_2) are approximated[17−19] by

$$C \leq \frac{E_2^3}{E_1^3} \exp\left(\frac{E_1 - E_2}{k_B T} \right) \tag{1}$$

Equation 1 indicates that C should increase exponentially with the difference in photon energies (often called the Stokes shift). According to eq 1, for a Stokes shift greater than 300 meV, C could exceed the geometric optical limit[20] of 46 200 for direct solar radiation.

Recent renewed interest in LSCs has been driven by materials research to overcome the reabsorption losses due to insufficient Stokes shifts, with particular emphasis on nanocrystal lumophores.[7] One such class of nanocrystals is the quantum dot heterostructure shown in Figure 1, where the effective Stokes shift can be controlled by tuning either the core size or the thickness of the larger band-gap shell.[21−23] As the shell-to-core volume ratio increases, the overlap between absorption and emission decreases, thereby reducing reabsorption losses for luminesced photons traveling through the waveguide.[21]

It has previously been shown that a wavelength-selective dielectric filter is thermodynamically required to achieve high efficiency.[24] Under idealized circumstances where the lumophore species has unity quantum yield, the polymer–lumophore matrix exhibits no scattering over the length scale of the concentrator, and the Stokes shift is large enough to allow for a high thermodynamic limit for C, the performance of

the LSC will still be limited by inefficient light guiding to the solar cell. In the traditional LSC design (Figure 1), the waveguide acts as a rudimentary wavelength-selective filter for photons: high-energy solar photons are refracted to subtend only a fraction of the solid angle inside the waveguide, whereas low-energy luminesced photons exist at all angles and accumulate inside the totally internally reflected modes.[19] The wavelength selectivity of this filter is inherently poor due to escape cone losses and can be improved with the addition of a wavelength-selective photonic mirror between the waveguide and the sun.[6,10,25]

Our strategy is to embed the lumophore in an optical cavity integrated with a carefully tuned wavelength-selective photonic mirror that transmits blue light and reflects red luminesced photons at all angles (Figure 1). Designer quantum dot materials offer an advantage over dye molecules in this regard. The emission spectra of nanocrystals are intrinsically narrower and more symmetric, enabling the design of a one-dimensional photonic mirror that operates omnidirectionally across the entire emission band. The design presented here targets high quantum yield, large Stokes shift, and narrow emission band CdSe/CdS core–shell nanocrystals with low scattering cross sections at the emission wavelength, combined with photonic structures that trap luminescence inside the waveguide.

■ RESULTS AND DISCUSSION

Although the Stokes shift of CdSe/CdS nanocrystals increases with increasing shell thickness, thereby reducing LSC losses, scattering between the nanoparticle and polymer matrix also increases with the volume and increases LSC losses. To find the optimal nanocrystal geometry, we synthesized CdSe/CdS nanoparticles with a constant 2.5 nm core diameter and varying shell thicknesses and compared the ratio of absorption at 450 nm to the extinction at the peak luminescence wavelength as shown in Figure 2a. For small shell thicknesses, the extinction is dominated by absorption in the CdSe core, whereas for large shell thicknesses the extinction is dominated by scattering between the nanoparticle and the waveguide polymer. The experimental results match well with theoretical calculations based on the electrostatic dipole model[26] using bulk refractive index data for CdSe and CdS.[27−30] For CdSe core sizes between 2 and 5 nm, there exists a maximum in the extinction ratio corresponding to a total particle diameter between 15 and 20 nm or total volume between 2000 and 4000 nm³. The particles chosen to make devices in this study have a 2.5 nm core and a 15.4 ± 1 nm total diameter, yielding an experimental extinction ratio of 230 to 1. A characteristic transmission electron micrograph is shown in Figure 1. The solution-phase luminescence quantum yield of the nanocrystals is 68%, and the luminescence is centered at 600 nm with a fwhm of 40 nm.

On the basis of the properties of these nanocrystals, we designed a wavelength-selective photonic mirror that accepts incident blue sunlight and traps luminescence. From 350 to 520 nm the photonic mirror exhibits 90% average transmission at normal incidence. Over the emission band of the lumophore, the hemispherically averaged reflectance of the mirror is 98%, with a maximum reflectivity of >99.999% at 650 nm at normal incidence. The dependence of reflectivity on angle of incidence is characterized in Figure 2b; luminesced photons are reflected efficiently up to 60 degrees from normal, with diminished reflectivity at higher angles. The photographs in Figure 2c show the effect of the photonic mirror on luminescence from the
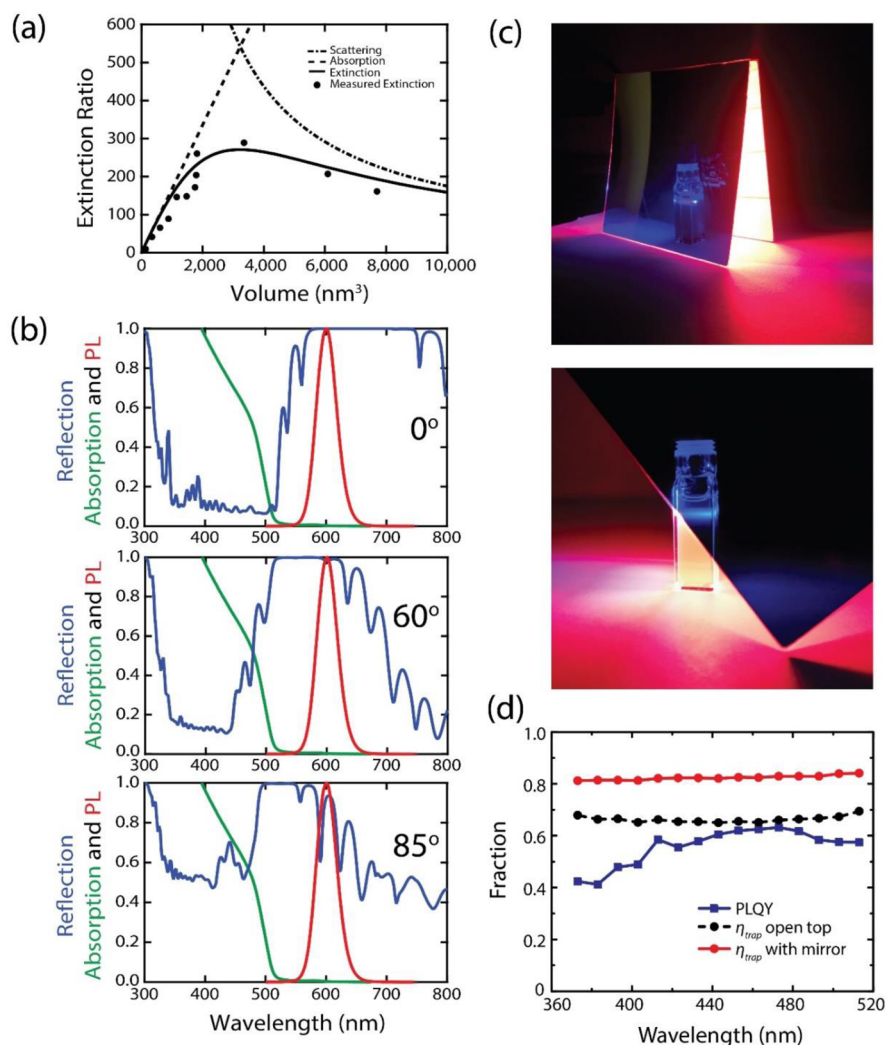
Figure 2. (a) Data and simulation of the relationship between shell volume and the ratio of extinction at 450 nm to extinction at 600 nm for CdSe/CdS core/shell nanoparticles with a 2.5 nm core diameter. The dashed lines represent the ratio of extinction at 450 nm to the absorption at 600 nm and scattering at 600 nm, as calculated by the electrostatic dipole approximation. The solid line is the ratio of the extinction at 450 nm to the sum of absorption and scattering at 600 nm. (b) Absorption and emission spectra of the QDs as compared to the reflectivity of the photonic mirror at different incidence angles. (c) Photographs of the QD solution under blue laser illumination with photonic mirrors reflecting the luminesced red light. (d) PLQY of the QD/PLMA film and the trapping efficiency before and after integration with the photonic mirror.

quantum dot solution under 440 nm excitation. In the first photograph, two mirrors are arranged in a tent over the cuvette and all luminescence is directed to the opening since it cannot pass through the mirror. In the second, the scattered blue laser light transmits through the mirror, while the luminescence from the lumophore solution is blocked.

The quantum dots are integrated into a poly(lauryl methacrylate) (PLMA) matrix to form an optically clear LSC waveguide. The photoluminescence quantum yields (PLQYs) of the nanocrystals decrease upon integration with the polymer, decreasing from 68% to 60% (Figure 2d). The effect of the photonic mirror was quantified by measuring the optical trapping efficiency (η_{trap}), the fraction of photons that propagate to the edges of the waveguide (i.e., no embedded solar microcell). Without the photonic mirror, η_{trap} is limited by the fraction (η_{TIR}) of photons initially trapped by total internal reflection in a polymer with refractive index n.

$$\eta_{trap} \leq \eta_{TIR} = (1 - n^{-2})^{1/2} \qquad (2)$$

For the PLMA/QD composite ($n = 1.44$), $\eta_{TIR} = 0.72$. For a 30 μm thick luminescent film placed between two thin glass coverslips, η_{trap} averages around 66% (Figure 2d), slightly lower than η_{TIR} due to scattering and reabsorption losses. Replacing both glass coverslips with photonic mirrors, luminesced photons cannot escape out of the front and back surface of the waveguide, increasing η_{trap} to 82% (Figure 2d), exceeding the value Snell's law would allow without the dielectric mirrors.

Figure 3a shows the concentrator cavity, consisting of the wavelength-selective photonic mirror on top, a PLMA/QD waveguide with an embedded Si solar microcell,[31,32] and a trench-shaped diffuse reflector that both enhances absorption of incident photons and recycles photons that escape through the bottom and edges of the waveguide. It is important to note that in this iteration the single Si microcell acts as a detector of the optical concentration. The overall EQE and collection efficiency of the device are low due to the small area covered by the single microcell. In the future, arrays of microcells could be integrated so as to capture more of the waveguided light with minimal shadowing. The best device performance under
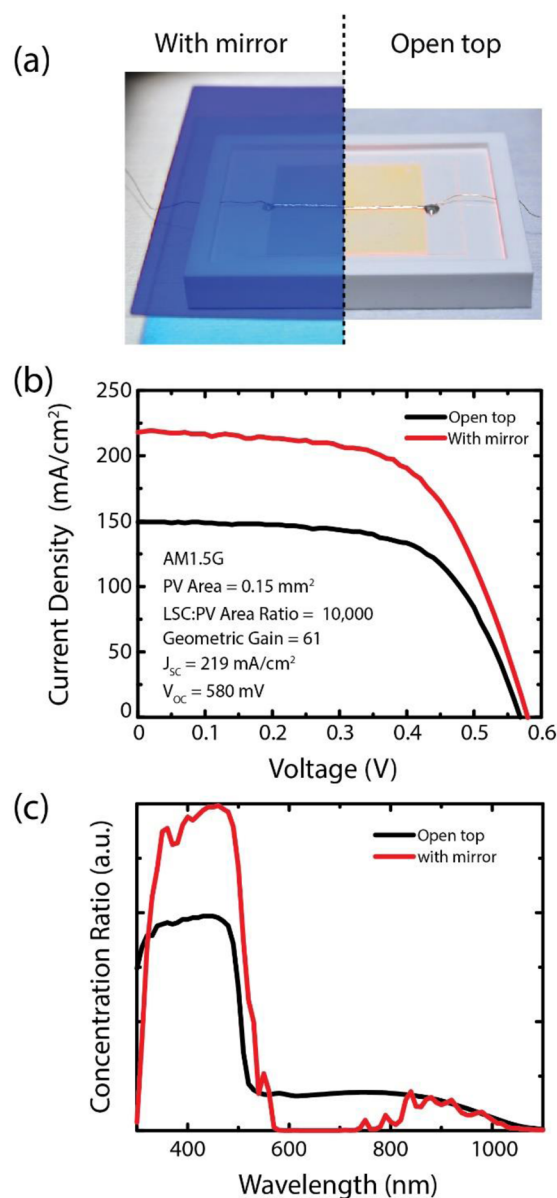
Figure 3. (a) Photograph of a microcell-LSC integrated with a photonic mirror and a trench-shaped diffuse trench reflector; (b) *J*–*V* characteristics of the LSC device with and without the photonic mirror; (c) concentration ratio as a function of excitation wavelength of the LSC-PV device with and without the photonic mirror.

plotted in Figure 3c and shows that the current enhancement originates from concentration of blue photons, the spectral region where the nanocrystals absorb. From 550 to 800 nm *C* is greatly suppressed, as this spectral region is reflected by the photonic mirror and prevented from entering the LSC. This loss is outweighed by the improvement in the concentration of blue photons as demonstrated by the total current enhancement.

The optical density (OD) at 450 nm of the nanocrystal–polymer films was then varied from 0.1 to 1.2, and the LSCs were characterized under blue-filtered illumination. The highest concentration factor occurs when OD = 0.65 (Figure 4a). At lower OD, absorption of incident sunlight in the blue portion of the spectrum is diminished, while at higher OD reabsorption and scattering of luminesced photons decrease the optical efficiency. All samples demonstrate more than 60% enhancement in *C* after applying the photonic mirror except the control device (no QDs added in the polymer). The optimum *C* under the blue-filter illumination with the photonic mirror reaches 30.3, a value unprecedented in the LSC literature.

To study the propagation of photons inside the LSC, we compared a sample with high internal scattering (Figure 4b, due to the absence of thorough QD cleaning before polymerization) to one with low scattering (Figure 4c) (see Supporting Method S4 for details). Both samples had an optimal OD of 0.65 at 450 nm and were measured under blue-filtered illumination with a variable illumination spot diameter, resulting in variable geometric gain *G* (the ratio of illuminated area to illuminated edge area; see Supporting equation S6 and Supporting discussion S5). Without the photonic mirror acting as a photon-recycling element, the sample with high scattering (Figure 4b) shows a limited growth of *C* that quickly plateaus with increasing *G*, as luminesced photons are scattered out of the waveguide and lost. In comparison, the sample with low scattering exhibits a quasi-linear increase of *C* with *G* (Figure 4c), as contributed by the uninterrupted TIR modes inside the waveguide.[21]

Adding the photonic mirror on top allows both non-TIR and scattered photons to be recycled and then to propagate inside the concentrator cavity before finally reaching the solar cell. As a result, the losses associated with scattering are strongly reduced, and photons are concentrated over distances much longer than the scattering length of the waveguide. In the high-scattering case (Figure 4b) *C* becomes quasi-linear with increasing *G* and reaches 16 at *G* = 37, nearly 5 times higher than without the mirror. This value is still smaller than that in the low-scattering case (*C* = 20), indicating that scattering loss is not completely mitigated as the mirror reflectivity diminishes at oblique angles. Measurement of the luminescent concentration factor of the high-scattering sample with the dielectric mirror at *G* = 61 resulted in *C* = 26, only slightly reduced from the best value of 30.3 for the nonscattering device. In the device with low scattering (Figure 4c), *C* increases superlinearly with the illumination diameter, increasing faster than the TIR limit
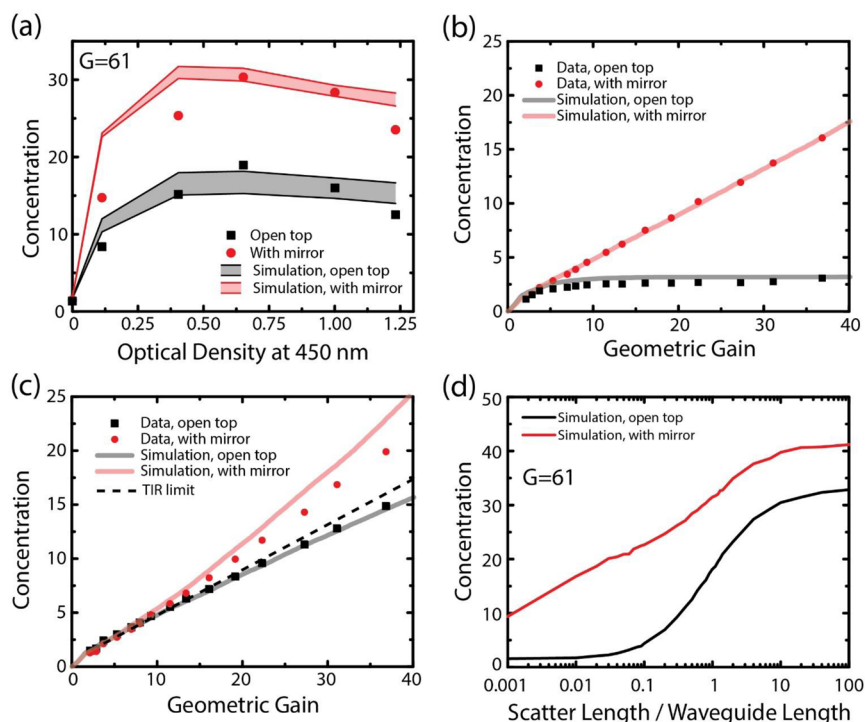
AM1.5G illumination is summarized in Table 1, with current density (*J*)–voltage (*V*) curves shown in Figure 3b. Both the *J*$_{sc}$ and the *V*$_{oc}$ of the microcell increase significantly upon integration with the LSC including the trench reflector and increase further with the addition of the photonic mirror. The total *J*$_{sc}$ of the Si microcell is 7.7 times higher after integration with the complete device. The spectral dependence of *C* is

Table 1. Summary of PV Device Performance before and after the Integration with the LSC, Trench Reflector, and Photonic Luminescence-Trapping Mirror under AM1.5G Illumination

testing condition	J_{sc} (mA/cm^2)	concentration λ = 350–500 nm	V_{oc} (V)	fill factor	power (mW/cm^2)
μ-Si device	28.51	1	0.504	0.72	10.35
μ-Si device with LSC with trench reflector	149.3	18.9	0.569	0.64	54.37
μ-Si device with LSC with trench reflector with photonic mirror	218.7	30.3	0.580	0.61	77.38

Figure 4. (a) Experimental and simulated photon concentration ratios at different optical densities of QD, with a geometric gain (*G*) of 61. The range of simulation results represent the best-fit range of scattering lengths, from 2.1 to 3.0 mm. Luminescence propagation data and simulation for (b) the highly scattering sample (with a scattering length of 0.18 mm) and (c) the record device (with a scattering length of 3 mm) compared to the limit imposed by total internal reflection (TIR). (d) Simulated effects of scattering length on concentration with and without a luminescence-trapping mirror, with *G* = 61.

imposed by eq 2. This superlinearity marks the onset of a transition from ballistic, single-pass photon transport to diffusion-based transport afforded by photon recycling. Our results suggest that efficient trapping of luminescence with a dielectric mirror can keep the luminescence inside the cavity regardless of the optical clarity and smoothness of the waveguide. If the optical quality of the waveguide could truly be made irrelevant by the dielectric mirror, the fabrication of the devices could be simplified.

To further investigate the connection between photon scattering, the photonic mirror, and *C*, we used a Monte Carlo ray tracing model. These simulations assume that scattering derives from the refractive index contrast between the nanocrystals and the PLMA waveguide. For each device, a range of scattering lengths are simulated and fit to the experimental data (Figure 4a). All other model inputs are measured experimentally. For the high- and low-scattering devices (Figure 4b,c), the best fit is achieved with 0.18 and 3 mm scattering lengths (Supporting method S7). A scattering length of 3 mm corresponds to roughly one scattering event for a photon propagating at 19 mm from the edge of the waveguide to the solar cell. Figure 4d shows the results of simulations systematically modeling the effect of scattering on device performance. Without the photonic mirror, *C* is negligible until the scattering length approaches the waveguide length and asymptotes when the scattering length is longer than the waveguide length. With the photonic mirror on top, the performance is less sensitive to the detrimental effects of scattering. However, the best results are still achieved when the scattering length is greater than the waveguide length.

CONCLUSION

In conclusion, the design presented here achieves luminescent solar concentration ratios over 30 while maintaining a high waveguide efficiency of 82%. This is due to the combination of designer nanocrystal lumophores with a photonic cavity that traps luminescence. The narrow emission line width of the nanocrystal lumophores enables the use of a highly reflective, wavelength-selective photonic mirror as the top surface of the cavity. In addition to improving the photon concentration ratio, the luminescence-trapping effect of the mirror also dramatically mitigates the detrimental effect of scattering.

The device fabricated here is tuned to utilize the blue portion of the spectrum due to the engineered absorption spectrum of the CdSe/CdS QDs. The system efficiency remains limited, as only one silicon microcell is utilized to detect rather than fully convert the luminescence in the waveguide. Using transfer-printing-based assembly, however, arrays of these microscale devices could be embedded in the waveguide to dramatically enhance the PV conversion efficiency.[33] Coupling with III−V (e.g., InGaP) microcell arrays with band gaps tailored to match QD emission, a luminescent concentrator cavity module could be constructed with efficiencies comparable to conventional PV panels but with reduced materials consumption. Additionally, this LSC module can be potentially used as the top layer (e.g., over Si) in a mechanically stacked multijunction architecture for full spectrum conversion, utilizing both the high-energy photons in the LSC and the low-energy photons in the bottom photovoltaic. We expect that future devices will achieve even higher concentration ratios while maintaining high waveguide efficiency through improvements to the luminescence quantum yield, waveguide geometry, and photonic mirror design.

METHODS

Quantum Dot Synthesis. CdSe quantum dots were synthesized following literature procedures. Details can be found in Supporting method S1.

Quantum Dot Characterization. Optical absorption spectra were taken on a Shimadzu UV-3600 absorption spectrometer. Fluorescence spectra were collected with a Jobin-Yvon FluoroLog 2, calibrated with an Ocean Optics HL3-plus radiometric calibration lamp and a Spectralon diffuse reflector from Lab Sphere.

Fluorescence quantum yields were measured on a custom integrating sphere fluorometer, as described in Supplementary method S2. To ensure proper quantitative measurement technique, the fluorescence quantum yield of rhodamine 590 in ethanol was measured and found to be 93.5%, reproducible to within 1%.

Transmission electron micrographs were obtained on a 200 kV Tecnai G220 S-TWIN with a Gatan SC200 CCD camera. Sizing was accomplished by analyzing the particles with an automated sizing algorithm (Supporting method S2).

Dielectric Mirror Design, Fabrication, and Analysis. The wavelength-selective dielectric mirror was designed and fabricated by Optical Filter Source, LLC (Austin, TX, USA). The reflectivity spectrum was measured by mounting a mirror on an optics post and measuring the transmittance as a function of angle. The average reflectivity is calculated by multiplying a normalized quantum dot luminescence spectrum $PL_{norm}(\lambda)$ by the reflectivity spectrum $R(\lambda,\theta)$ and integrating over a hemispherical emission, following eq 3. Details can be found in Supporting method S3.

$$R_{av} = \int_0^\pi \int_\lambda R(\lambda, \theta) \, PL_{norm}(\lambda) \, d\lambda \, \cos(\theta) \, \sin(\theta) \, d\theta \tag{3}$$

Luminescent Waveguide Fabrication and Characterization. The monomer lauryl methacrylate (LMA, Sigma-Aldrich) and the cross-linker ethylene glycol dimethacrylate (EGDMA, Sigma-Aldrich) were first purified to remove the inhibitor and then mixed at a 10:1 volume ratio. The CdS/CdSe quantum dots were then dispersed in this solution and polymerized under UV illumination (365 nm) and inert atmosphere with Darocur 1173 (Sigma-Aldrich) added as the initiator (1% by volume).

The film absorption was measured using a Varian Cary 5G spectrophotometer. The photoluminescence quantum yields (PLMA) and optical trapping efficiency (η_{trap}) of the waveguide were measured in a custom setup, as detailed in Supporting method S4.

Device Fabrication and Characterization. Monocrystalline silicon microcells (30 μm thick, 100 μm wide, and 1500 μm long) with a thermal oxide passivation layer were fabricated using photolithography, reactive ion etching, and wet chemical etching from p-type (111) Czochralski Si wafers (10 Ω·cm, Silicon Materials Inc.), as reported previously. The resulting devices were transfer-printed individually onto a glass substrate (170 μm thick) with a thin (~30 μm), partially cured adhesive (NOA61, Norland Products) layer. A 1.5 in. square quartz plate, treated with repel silane (GE Healthcare), was placed on top of the device. The microcell was then embedded in the luminescent waveguide (30 μm thick) through capillary filling of the LMA/QD solution and subsequent polymerization. The film thickness (30 μm) was controlled by using soda lime glass spacers (SPI product #2714) at the corners of the substrate.

After removing the quartz plate, the interconnects of the device were formed by screen-printing silver epoxy (E4110, Epo-Tek) lines and curing at room temperature.

The photovoltaic characteristics of the microcells in the concentrator cavity were measured using a source meter (model 2400, Keithley) and a 1000 W full spectrum solar simulator (Oriel, 91192) with an AM1.5 G filter. The concentration ratio (au) as a function of excitation wavelength was measured using an OL-750 automated spectroradiometric system (Gooch & Housego). The LSC device was placed inside a trench diffuse reflector (Spectralon, Labsphere) at all these measurements, while the PV performance of the microcell before integrating with the concentrator cavity was measured on a nonreflective substrate.

The propagation curve was obtained by placing a circular iris diaphragm (Newport) on top of the waveguide with the solar cell located in the center. The photocurrent was measured with a blue filter (Hoya 390) under the solar simulator while changing the illumination area with the diaphragm aperture size. The concentration factor C is calculated from the short-circuit current density J_{LSC} in mA cm^{-2} by

$$C = \frac{J_{LSC}}{\int T(\lambda) \, AM1.5G(\lambda) \, d\lambda \, EQE_{device}(600 \text{ nm})} \tag{4}$$

where $T(\lambda)$ is the transmission spectrum of the Hoya 390 filter, $AM1.5G(\lambda)$ is the solar spectrum flux in mA cm^{-2} nm^{-1}, and $EQE_{device}(600 \text{ nm})$ is the EQE of the silicon photovoltaic device measured on a nonreflective substrate at the emission wavelength (600 nm). Further details can be found in Supporting method S6.

ASSOCIATED CONTENT

S **Supporting Information**

The Supporting Information is available free of charge on the ACS Publications website at DOI: 10.1021/acsphotonics.5b00334.

> Synthesis, cleaning, and characterization of quantum dots. Characterization of reflectance spectrum of photonic mirror. Optical characterization of quantum dot polymer composite films. Definition of geometric gain and discussion thereof. Photovoltaic characterization of luminescent concentrator devices. Monte Carlo simulations of luminescent concentrator devices (PDF)

AUTHOR INFORMATION

Corresponding Authors
*E-mail: alivis@berkeley.edu.
*E-mail: r-nuzzo@illinois.edu.

Author Contributions
N.D.B., Y.Y., L.X., V.E.F., R.G.N., and A.P.A. wrote the manuscript. N.D.B., A.S.P., and E.O. synthesized and analyzed nanocrystals. N.D.B. and V.E.F. performed the electrodynamic simulations. Y.Y. and L.X. fabricated the luminescent waveguides and photovoltaic devices. Y.Y. and L.X. assembled the LSC device and performed its optical and electrical characterizations. N.D.B. and A.S.P. wrote and performed device simulations. A.P.A. and R.G.N. provided guidance.

Author Contributions
¶N. D. Bronstein, Y. Yao, and L. Xu contributed equally to this work.

■ REFERENCES

(1) Batchelder, J. S.; Zewail, A. H.; Cole, T. Luminescent Solar Concentrators. 1: Theory of Operation and Techniques for Performance Evaluation. *Appl. Opt.* **1979**, *18*, 3090−3110.

(2) Batchelder, J. S.; Zewail, A. H.; Cole, T. Luminescent Solar Concentrators. 2: Experimental and Theoretical Analysis of Their Possible Efficiencies. *Appl. Opt.* **1981**, *20*, 3733−3754.

(3) Goetzberger, A.; Greube, W. Applied Physics Solar Energy Conversion with Fluorescent Collectors. *Appl. Phys.* **1977**, *14*, 123−139.

(4) Weber, W. H.; Lambe, J. Luminescent Greenhouse Collector for Solar Radiation. *Appl. Opt.* **1976**, *15*, 3−4.

(5) Debije, M. G.; Verbunt, P. P. C. Thirty Years of Luminescent Solar Concentrator Research: Solar Energy for the Built Environment. *Adv. Energy Mater.* **2012**, *2*, 12−35.

(6) Goldschmidt, J. C.; Peters, M.; Gutmann, J.; Steidl, L.; Zentel, R.; Bläsi, B.; Hermle, M.; Chemie, O.; Mainz, U. Increasing Fluorescent Concentrator Light Collection Efficiency by Restricting the Angular Emission Characteristic of the Incorporated Luminescent Material - the "Nano-Fluko" Concept. *Proc. SPIE* **2010**, *7725*, 77250.

(7) Bradshaw, L. R.; Knowles, K. E.; McDowall, S.; Gamelin, D. R. Nanocrystals for Luminescent Solar Concentrators. *Nano Lett.* **2015**, *15*, 1315−1323.

(8) Chatten, A. J.; Barnham, K. W. J.; Buxton, B. F.; Ekins-Daukes, N. J.; Malik, M. A. Quantum Dot Solar Concentrators. *Semiconductors* **2004**, *38*, 909−917.

(9) Debije, M. G.; Teunissen, J.-P.; Kastelijn, M. J.; Verbunt, P. P. C.; Bastiaansen, C. W. M. The Effect of a Scattering Layer on the Edge Output of a Luminescent Solar Concentrator. *Sol. Energy Mater. Sol. Cells* **2009**, *93*, 1345−1350.

(10) Debije, M. G.; Van, M.-P.; Verbunt, P. P. C.; Kastelijn, M. J.; van der Blom, R. H. L.; Broer, D. J.; Bastiaansen, C. W. M. Effect on the Output of a Luminescent Solar Concentrator on Application of Organic Wavelength-Selective Mirrors. *Appl. Opt.* **2010**, *49*, 745−751.

(11) Krumer, Z.; Pera, S. J.; van Dijk-Moes, R. J. A.; Zhao, Y.; de Brouwer, A. F. P.; Groeneveld, E.; Van Sark, W. G. J. H. M.; Schropp, R. E. I.; de Mello Donegá, C. Tackling Self-Absorption in Luminescent Solar Concentrators with Type-II Colloidal Quantum Dots. *Sol. Energy Mater. Sol. Cells* **2013**, *111*, 57−65.

(12) Roncali, J.; Garnier, F. Photon-Transport Properties of Luminescent Solar Concentrators: Analysis and Optimization. *Appl. Opt.* **1984**, *23*, 2809.

(13) Bomm, J.; Büchtemann, A.; Chatten, A. J.; Bose, R.; Farrell, D. J.; Chan, N. L. A.; Xiao, Y.; Slooff, L. H.; Meyer, T.; Meyer, A.; et al. Fabrication and Full Characterization of State-of-the-Art Quantum Dot Luminescent Solar Concentrators. *Sol. Energy Mater. Sol. Cells* **2011**, *95*, 2087−2094.

(14) Van Sark, W. G. J. H. M.; Barnham, K. W. J.; Slooff, L. H.; Chatten, A. J.; Büchtemann, A.; Meyer, A.; McCormack, S. J.; Koole, R.; Farrell, D. J.; Bose, R.; et al. Luminescent Solar Concentrators–a Review of Recent Results. *Opt. Express* **2008**, *16*, 21773−21792.

(15) Giebink, N. C.; Wiederrecht, G. P.; Wasielewski, M. R. Resonance-Shifting to Circumvent Reabsorption Loss in Luminescent Solar Concentrators. *Nat. Photonics* **2011**, *5*, 694−701.

(16) Roncali, J.; Garnier, F. New Luminescent Back Reflectors for the Improvement of the Spectral Response and Efficiency of Luminescent Solar Concentrators. *Sol. Cells* **1984**, *13*, 133−143.

(17) Yablonovitch, E. Thermodynamics of the Fluorescent Planar Concentrator. *J. Opt. Soc. Am.* **1980**, *70*, 1362.

(18) Smestad, G.; Ries, H.; Winston, R.; Yablonovitch, E. The Thermodynamic Limits of Light Concentrators. *Sol. Energy Mater.* **1990**, *21*, 99−111.

(19) Ries, H.; Smestad, G. P.; Winston, R. Thermodynamics of Light Concentrators. *Proceedings of SPIE* **1991**, *1528*, 7.

(20) Wurfel, P. *Physics of Solar Cells*, 2nd ed.; Wiley-VCH Verlag Gmbh & Co. KGaA: Weinheim, 2009.

(21) Bronstein, N. D.; Li, L.; Xu, L.; Yao, Y.; Ferry, V. E.; Alivisatos, A. P.; Nuzzo, R. G. Luminescent Solar Concentration with Semiconductor Nanorods and Transfer-Printed Micro-Silicon Solar Cells. *ACS Nano* **2014**, *8*, 44−53.

(22) Meinardi, F.; Colombo, A.; Velizhanin, K. A.; Simonutti, R.; Lorenzon, M.; Beverina, L.; Viswanatha, R.; Klimov, V. I.; Brovelli, S. Large-Area Luminescent Solar Concentrators Based on "Stokes-Shift-Engineered" Nanocrystals in a Mass-Polymerized PMMA Matrix. *Nat. Photonics* **2014**, *8*, 392−399.

(23) Coropceanu, I.; Bawendi, M. G. Core/shell Quantum Dot Based Luminescent Solar Concentrators with Reduced Reabsorption and Enhanced Efficiency. *Nano Lett.* **2014**, *14*, 4097−4101.

(24) Rau, U.; Einsele, F.; Glaeser, G. C. Efficiency Limits of Photovoltaic Fluorescent Collectors. *Appl. Phys. Lett.* **2005**, *87*, 1−3.

(25) Slooff, L. H.; Burgers, A. R.; Debije, M. G. Reduction of Escape Cone Losses in Luminescent Solar Concentrators with Cholesteric Mirrors. *Proc. SPIE* **2008**, *7043*, 704306−704306−7.

(26) Bohren, C. F.; Huffman, D. R. *Absorption and Scattering of Light by Small Particles*; Wiley-VCH Verlag GmbH & Co. KGaA: Weinheim, 1983.

(27) Palik, E. D. *Handbook of Optical Constants of Solids*; Academic Press: Burlington, 1997.

(28) Jasieniak, J.; Smith, L.; van Embden, J.; Mulvaney, P. Re-Examination of the Size-Dependent Absorption Properties of CdSe Quantum Dots. *J. Phys. Chem. C* **2009**, *113*, 19468−19474.

(29) Ninomiya, S.; Adachi, S. Optical Properties of Wurtzite. *J. Appl. Phys.* **1995**, *78*, 1183−1190.

(30) Moreels, I.; Allan, G.; De Geyter, B.; Wirtz, L.; Delerue, C.; Hens, Z. Dielectric Function of Colloidal Lead Chalcogenide Quantum Dots Obtained by a Kramers-Krönig Analysis of the Absorbance Spectrum. *Phys. Rev. B: Condens. Matter Mater. Phys.* **2010**, *81*, 235319.

(31) Yao, Y.; Brueckner, E.; Li, L.; Nuzzo, R. Fabrication and Assembly of Ultrathin High-Efficiency Silicon Solar Microcells Integrating Electrical Passivation and Anti-Reflection Coatings. *Energy Environ. Sci.* **2013**, *6*, 3071.

(32) Yoon, J.; Baca, A. J.; Park, S.-I.; Elvikis, P.; Geddes, J. B.; Li, L.; Kim, R. H.; Xiao, J.; Wang, S.; Kim, T.-H.; Motala, M. J.; Ahn, B. Y.; Duoss, E. B.; Lewis, J. A.; Nuzzo, R. G.; Ferreira, P. M.; Huang, Y.; Rockett, A.; Rogers, J. A. Ultrathin Silicon Solar Microcells for Semitransparent, Mechanically Flexible and Microconcentrator Module Designs. *Nat. Mater.* **2008**, *7*, 907−915.

(33) Yoon, J.; Li, L.; Semichaevsky, A. V.; Ryu, J. H.; Johnson, H. T.; Nuzzo, R. G.; Rogers, J. A. Flexible Concentrator Photovoltaics Based on Microscale Silicon Solar Cells Embedded in Luminescent Waveguides. *Nat. Commun.* **2011**, *2*, 343.